Research Article Vol. 30, No. 3 / 31 Jan 2022 / Optics Express 3675
Optics EXPRESS

Light detection and ranging with entangled photons

JIUXUAN ZHAO,[1] ASHLEY LYONS,[2] ARIN CAN ULKU,[1] HUGO DEFIENNE,[2] DANIELE FACCIO,[2,3] AND EDOARDO CHARBON[1,4]

[1]*Advanced Quantum Architecture Laboratory (AQUA), Ecole Polytechnique Federale de Lausanne (EPFL), 2002 Neuchatel, Switzerland*
[2]*School of Physics and Astronomy, University of Glasgow, Glasgow G12 8QQ, UK*
[3]*daniele.faccio@glasgow.ac.uk*
[4]*edoardo.charbon@epfl.ch*

Abstract: Single-photon light detection and ranging (LiDAR) is a key technology for depth imaging through complex environments. Despite recent advances, an open challenge is the ability to isolate the LiDAR signal from other spurious sources including background light and jamming signals. Here we show that a time-resolved coincidence scheme can address these challenges by exploiting spatio-temporal correlations between entangled photon pairs. We demonstrate that a photon-pair-based LiDAR can distill desired depth information in the presence of both synchronous and asynchronous spurious signals without prior knowledge of the scene and the target object. This result enables the development of robust and secure quantum LiDAR systems and paves the way to time-resolved quantum imaging applications.

1. Introduction

Light detection and ranging (LiDAR) systems with the ability to reach long distance at high speed and accuracy have emerged as a key technology in autonomous driving, robotics, and remote sensing [1]. Today miniaturised LiDARs are integrated in many consumer electronics devices, e.g. smartphones. Moving beyond depth sensing, the LiDAR technique has been also used for non-line-of-sight imaging [2–6], imaging through scattering media [7] and biophotonics applications [8]. A typical LiDAR system records the time-of-flight, t, of light back-reflected from a scene, which enables to estimate distance $d = ct/2$, where c is the speed of light [9]. Thanks to their single-photon sensitivity, picosecond temporal resolution and low cost, single-photon avalanche diodes (SPADs) are widely used as detectors in LiDAR [10,11]. In this respect, two well established techniques can be used to achieve the timing information at picosecond resolution: time-correlated single-photon counting (TCSPC) that operates by recording a time-stamp for each individual photon [12–14] or time gating in which a gate window is finely shifted [15–18].

Despite recent advances, interference is a major challenge for robust and secure LiDAR applications through complex environments. In our work, the term 'interference' refers to the detection by the LiDAR sensor of any optical signals other than those emitted by the LiDAR source. These may originate from ambient light, other LiDAR systems operating concurrently and intentional spoofing signals. In addition to depth distortion such as degradation in accuracy and precision, interference could result in misleading information, causing the system to make incorrect decisions. Over the past several years, some approaches addressing LiDAR interference have been proposed. One technique isolates the signal based on temporal correlations between two or more photons [19], which effectively suppresses noise due to ambient light. Another technique based on laser phase modulation can reduce both ambient light and mutual interference [13,14]. However, these approaches have limitations. For example, an external signal can

#435898 https://doi.org/10.1364/OE.435898
Journal © 2022 Received 2 Jul 2021; revised 22 Dec 2021; accepted 8 Jan 2022; published 20 Jan 2022

Optics EXPRESS

still spoof the LiDAR detector if it copies the temporal correlation or phase modulation of the illumination source, which is easily achievable by placing a photodiode close to the target object. To date, there is no LiDAR system immune to all types of interference.

The use of non-classical optical states can also improve object detection in the presence of spurious light and noise. In a quantum illumination protocol, a single photon is sent out towards a target object while its entangled pair is retained and used as an ancilla [20]. Coincidence detection between the returned photon and its twin increases the effective signal-to-noise ratio compared to classical illumination, an advantage persisting even in the presence of noise and losses. Recently, practical quantum illumination schemes have been experimentally demonstrated using spatially entangled photon pairs for target detection [21,22] and imaging objects [23–25] in the presence of background light and spurious images. These approaches rely on the ability to measure photon coincidences between many spatial positions, which is conventionally performed using single-photon sensitive cameras such as electron multiplied charge coupled device (EMCCD) cameras [26–28], intensified(i)CCD [29,30] and SPAD cameras [31–34]. However, while a handful of works have reported the use of photon pairs for target detection at distance [35–37], no imaging LiDAR experiments with absolute range distance and interference or background rejection have been reported.

In this work, we demonstrate a quantum LiDAR system immune to any type of classical interference, with the exception of blinding attacks [38], by using a pulsed light source of spatially entangled photon pairs and a time-resolved SPAD camera. We use spatial anti-correlations between photon pairs as a unique identifier to distinguish them from any other light sources in the target scene. In particular, we show how our LiDAR system successfully images objects and retrieves their depths in two different interference scenarios mimicking the presence of spoofing or additional classical LiDAR signals. In the first case, spurious light from a synchronised laser is used to demonstrate the robustness against intentional spoofing attacks. In the second case, the interference takes the form of asynchronous pulses imitating the presence of multiple background LiDAR systems running in parallel. The results show that our approach enables to image with high depth resolution while offering immunity to classical light interference.

2. Imaging system

The experimental setup is shown in Fig. 1(a). Spatially entangled photon pairs are produced by type-I spontaneous parametric down conversion (SPDC) with a β-Barium Borate (BBO) nonlinear crystal pumped by a 355 nm pulsed laser with a repetition frequency of 20 MHz. The objects to be imaged are masks placed on a reflective mirror. One object O_1 ("skater") is placed in the far field of the crystal thus the down-converted photon pairs are spatially anti-correlated at the object plane. Another object O_2 ("car") is illuminated by a diffused 780 nm laser pulsed at 20 MHz as well to produce the interference. Both objects are imaged onto the SPAD camera *SwissSPAD2* [15] (see Supplement 1). Similar to a typical LiDAR scheme, the pump laser is synchronised with the camera, while the spoofing signal generated by a classical pulse laser can be synchronous or asynchronous.

As in conventional time-gated LiDAR, backscattered photons with specific time-of-flight are detected by scanning a gate window (15 ns wide) using 18 ps time steps, which corresponds to a depth resolution of 2.7 mm [15,16]. At each gate position, a set of 8-bit frames ($\sim 10^3$ frames) is acquired to reconstruct two different types of images: (i) a classical intensity image, obtained by summing all the frames, and (ii) a spatially-averaged photon correlation image computed by identifying photon coincidences in the frame set using a technique detailed in [28] (see Supplement 1). The intensity image retrieves the shape of the objects in the scene at a given depth, while the spatially-averaged correlation image measures spatial correlations between detected photons to identify the presence of photon pairs. For example, if only reflected photon pairs are captured within the gate window (Fig. 1(b)), the intensity image shows the "skater"

Optics EXPRESS

object and an intense peak is observed at the center of the spatially-averaged correlation image. The presence of such a correlation peak above the noise level confirms the presence of photon pairs among the detected photons. If only classical light is detected (Fig. 1(c)), the intensity images show the "car" object illuminated by the pulse laser and the spatially-averaged correlation image is flat.

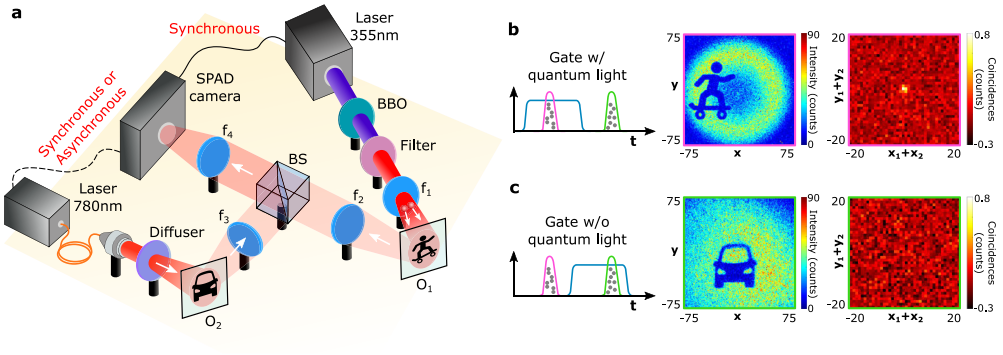

Fig. 1. Experimental setup and principle. **(a)** An object O_1 placed in the far field of a 1-mm-thick β-Barium Borate (BBO) nonlinear crystal is illuminated by spatially entangled photon pairs produced via type-I spontaneous parametric down conversion (SPDC), while an object O_2 is illuminated by diffused classical light. A lens $f_1 = 50$ mm is positioned after the crystal to direct the photon-pairs towards O_1. Both objects are composed of an absorptive pattern layer on a reflective surface. They are imaged onto the SPAD camera using lens $f_2 = 100$ mm, $f_3 = 50$ mm, $f_4 = 100$ mm and an unbalanced beam splitter (0.1R/0.9T). **(b)** When the SPAD gate window is set to capture only photon pair pulses reflected by the quantum object, the "skater-shape" object appears in the intensity image and a peak is detected in the spatially-averaged correlation image, which shows the number of photon coincidences spatially averaged over all pair of pixels r_1 and r_2 separated by a given distance $r_1 + r_2$. The correlation peak confirms the presence of photon pairs among the detected photons. **(c)** When the SPAD gate window is set to capture only classical light, the "car-shape" object appears in the intensity image whereas no peak obtained is visible in the spatially-averaged correlation image. Intensity and spatially-averaged correlation images were reconstructed from $N = 2000$ frames (8-bit) acquired using an exposure time of 350 ns (1-bit). Intensity image coordinate units are in pixels.

3. Synchronous classical light interference

First, we consider the case of a spurious classical source of light that is synchronised with the SPAD camera i.e. photons reflected by both O_1 ("person") and O_2 ("bike") are synchronous with the camera (Fig. 2(a)). This scenario corresponds to a spoofing attack. To operate the LiDAR, the gate window is continuously shifted over a range of 27 ns, which corresponds to 1500 gate positions. Figure 2(b) shows the intensity and spatially-averaged correlation images (zoom 9×9 pixels in inset) measured at four specific gate positions 0.09 ns, 7.2 ns, 14.58 ns and 23.4 ns. At the early gate position (0.09 ns), there is only noise recorded by the camera such as dark count, crosstalk, afterpulsing and ambient light. As the gate window is shifted, O_2 appears in the intensity image (7.2 ns) and the absence of a peak in the spatially-averaged correlation image shows that it originates from classical light alone. When the reflected quantum light starts to be collected in the gate window together with the classical light (14.58 ns), O_1 and O_2 are superposed in the intensity image and a correlation peak becomes visible. For the late gate window (23.4 ns) the classical laser pulse vanishes while only quantum light is detected, as

Optics EXPRESS

shown by the peak persisting in the spatially-averaged correlation image, and only O_1 is visible in the intensity image.

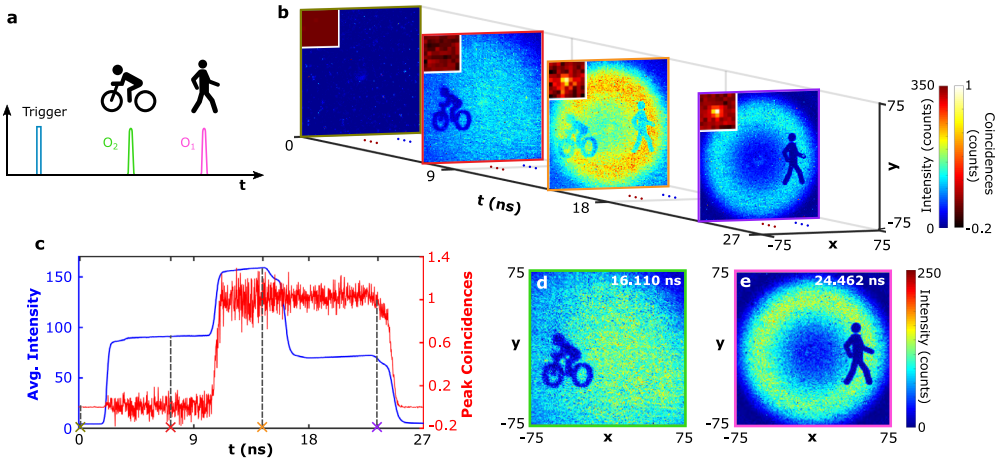

Fig. 2. Results with synchronous classical light interference. **(a)** The reflected light from objects O_1 ("person") and O_2 ("bike") are both synchronous with the camera. **(b)** shows the selected intensity and spatially-averaged correlation images (9×9 central data) at the gate positions 0.09 ns, 7.2 ns, 14.58 ns and 23.4 ns covered with none reflected light, reflected light from only O_1, O_1 & O_2, and only O_2 respectively. Correlation peaks are obtained at 14.58 ns and 23.4 ns gate positions when there is quantum light reflected to the camera. The measurement is implemented over a time range of 27 ns corresponding to 1500 continuous gate positions with a proper time offset initially to the pump laser trigger. **(c)** Average intensity over all pixels (blue curve) and the peak coincidences (red curve) values along the measured time range. The peak coincidences are the normalized coincidence values at the center position (0, 0) of the spatially-averaged correlation images. The four positions in **(b)** are also marked on the horizontal axis of the curve. **(d)** The subtracted intensity image of O_2 (classical) and its arrival time (16.110 ns) to the camera by locating the first falling edge of the average intensity profile. **(e)** The subtracted intensity image of O_1 (quantum) and its arrival time (24.462 ns) to the camera by locating the falling edge of the correlation peak profile. Experiments are performed by N = 5000 frames (8-bit) acquired in 13.5 s at each gate position using an exposure time of 350 ns for 1-bit frame. The time step between two successive gate windows is 18 ps. Intensity image coordinate unites are in pixels. See Visualization 1 for the entire scanning results.

To acquire depth information and distinguish classical interference, the spatially-averaged intensity and correlation peak values represented in function of the gate position in Fig. 2(c) are analyzed. The two-step average intensity profile represents the double reflections from O_1 and O_2, while the correlation peak profile only reveals the trend of quantum light over the given time range. By locating the falling edges of the intensity profile, the arrival time information of all the objects can be obtained [18,39]. Whilst by just searching for the last falling edge of the correlation peak profile, the arrival time information of the quantum object is extracted. As shown in Fig. 2(d), the arrival time of the classical object of 16.110 ns and its intensity image are obtained. The arrival time of the quantum object, 24.462 ns, is located at the last fitted falling edge of the correlation peak profile and the corresponding intensity image is subtracted in Fig. 2(e). Refer to Visualization 1 for the scanned results over the entire detected range. The proposed dual-profile locating method enables locating and distinguishing objects illuminated by quantum light or classical light.

Optics EXPRESS

The anti-spoofing capability works as described, as long as the time delay between the two objects is larger than the temporal resolution of the SPAD camera. One may then enhance the removal of temporally overlapping interferences by increasing the number of frames (e.g. up to $\sim 10^6$ 8-bit frames) for each gate delay so as to retrieve a spatially-resolved correlation image instead of a spatially-averaged correlation image [24,25,28,34]. An example is shown in Fig. 3: a spatially-resolved correlation image retrieves directly the shape of the object illuminated by photons pairs and remains insensitive to classical interference (classical background noise added in the experiment). In fact, such a spatially-resolved correlation image could potentially be measured at all gate positions of the LiDAR scanning. However, the acquisition time is much longer than that required to retrieve a spatially-averaged correlation image (a few hours instead of seconds for a single time gate delay) and it is therefore better to limit its use to gate positions for which the objects cannot be distinguished otherwise. In addition, note that because of the anti-symmetric spatial structure of photon pairs illuminating the object, each spatially-resolved correlation image contains both the object and its symmetric image, which means that the object must interact with only half of the photon pair beam to be imaged through correlations without ambiguity.

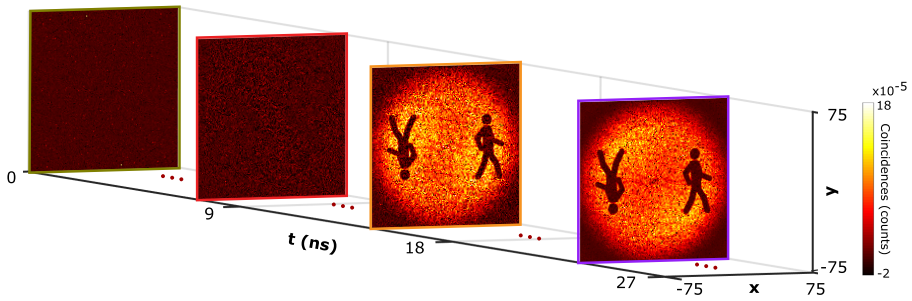

Fig. 3. Measurement of spatially-resolved correlation images over time. The shape of the object illuminated by photon pairs ("person") is retrieved by measuring spatially-resolved correlation images at the gate positions 0.09 ns, 7.2 ns, 14.58 ns and 23.4 ns. Each image is obtained by acquiring 5 million frames (8-bit), which corresponds to approximately 3.8 hours of acquisition.

4. Asynchronous classical light interference

In real-world applications, another possible scenario is the interference coming from ambient light and other LiDAR systems. We therefore consider a classical source of light that is not synchronised with the SPAD camera but still running at the same repetition frequency (20 MHz) and illuminates the object O_2 "50 traffic sign" (Fig. 4(a)). Figure 4(b) shows the intensity and correlation images at three example gate positions 2.16 ns, 13.5 ns and 24.66 ns. The object O_2 is visible in the intensity images at all gate positions as background noise. When the gate is shifted to 13.5 ns, the SPAD also captures photon pairs reflected by O_1 ("STOP traffic sign") and both objects are superimposed in the intensity image. We now also observe a peak in the spatially-averaged correlation image which highlights the presence of photon pairs. By locating the falling edge of the spatially-averaged correlation peak shown in Fig. 4(c), the time arrival information of the quantum object is located at 20.682 ns, and its intensity image is also obtained by subtraction as shown in Fig. 4(d). See Visualization 2 for the entire measured results.

Optics EXPRESS

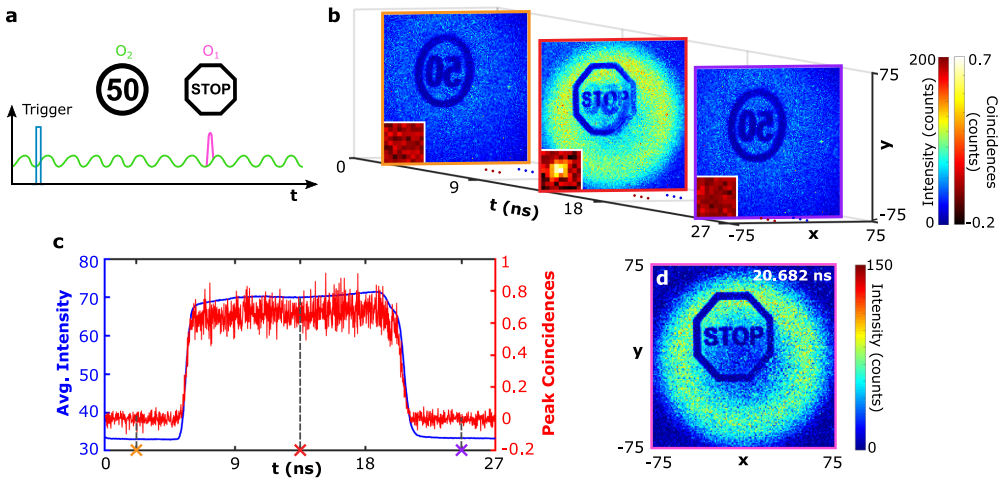

Fig. 4. Results with asynchronous spurious light. **(a)** Photon pairs reflected by object O_1 ("STOP traffic sign") is synchronous with the camera, while classical photons reflected by O_2 ("50 traffic sign") arrives at the camera in temporally random sequences as the classical laser is asynchronous. **(b)** The camera scanned over a time range of 27 ns (1500 continuous gate positions). Intensity and spatially-averaged correlation images (central 9×9 pixels area) are shown for three different gate positions (2.16 ns, 13.5 ns and 24.66 ns). The correlation peak only appears at the gate window covered with photon pairs reflected by O_1. **(c)** The corresponding three gate positions are marked in the curve of the average intensity and correlation peak responses over the detected time range. **(d)** Intensity image reconstructed by subtracting intensity image at 13.5 ns by this at 24.66 ns. At each gate position, $N = 3000$ frames (8-bit) were acquired in 8.1 s using an exposure time of 350 ns (1-bit). The time step between two successive gate positions is 18 ps. Intensity image coordinate unites are in pixels. See Visualization 2 for the entire scanning results.

5. Conclusion

We demonstrated a LiDAR system based on spatially entangled photon pairs showing robustness against interference from classical sources of light. In particular, we showed its successful use in the presence of (i) a spoofing attack (synchronous classical light interference) and (ii) of a background light and another LiDAR system operating in parallel (asynchronous classical light interference). Note also that because the quantum LiDAR harnesses anti-correlations between photon pairs to retrieve images, it is also immune to classically-correlated sources of light such as thermal and pseudo-thermal sources in which photons are position-correlated [40].

In our current implementation, time gate position is acquired in several seconds so that the full scanning takes several hours (5.6 hours for the synchronous case and 3.4 hours for the asynchronous case). This total acquisition time can however be significantly decreased by reducing (i) the acquisition time per gate position and (ii) the number of gate positions to detect the falling edge of quantum light (currently 1500 steps scanned linearly). For example, in the case of the synchronous classical light shown in Fig. 2, the quantum illuminated object could be located by measuring only 300 frames for 8 different gate positions by using a correlation-driven scanning and falling edge fitting algorithm, which would reduce the total acquisition time to 7 seconds (see details in the Supplement 1). In addition, the speed of the SPAD camera in our experiment was limited to 370 fps by the readout architecture, but it has been demonstrated that the similar cameras can be operated at frame rates up to 800, 000 fps [41], which would further diminish the total acquisition time and potentially reach real-time acquisition. Furthermore, in the current quantum LiDAR prototype the target object is a two dimensional 'co-operative' object

Optics EXPRESS

attached to a mirror, which ensures enough photon pairs are reflected and collected by the camera. However, the proposed scheme can be extended to scattering materials with three dimensional profiles by using brighter photon pair sources and more sensitive SPAD cameras, which are currently under development. For example, the photon pair source can generate approximately 610k photon pairs per second in our current experiment. However, the camera detects about 2.3 pairs of correlated photons at maximum per frame due to the low quantum efficiency (~6.5%) and the dead time (10.2 μs per bit) during readout, which can be improved dramatically. Looking forward, these results could enable the development of robust and secure LiDAR systems and more general time-resolved quantum imaging applications.

We note that generally speaking, it is unlikely that any form of quantum LiDAR will displace existing LiDAR technology for the simple reason that even single photon detection LiDAR still requires illumination with powerful laser pulses in order to compensate for the very large return losses incurred in long distance scenarios. Rather, a promising direction is that in which quantum LiDAR provides a different functionality beyond simple 3D scene imaging by adding, for example as shown here, an anti-spoofing approach that will work against other classical LiDAR systems. Other schemes have also been proposed that promise full anti-spoofing even against other quantum systems, verging more towards full scale quantum security protocols. Our scheme does not provide this additional level of security but it does provide the practical advantage of not requiring technologically challenging scanning delay lines for cross-correlating signal and idler photons that are part of the quantum-secure approaches [22,36].

Funding. Royal Academy of Engineering (EP/T00097X/1); H2020 Marie Skłodowska-Curie Actions (840958); H2020 Marie Skłodowska-Curie Actions (754354); Engineering and Physical Sciences Research Council (EP/R030081/1).

Acknowledgments. DF acknowledges financial support from the Royal Academy of Engineering under the Chairs in Emerging Technologies scheme and the UK Engineering and Physical Sciences Research Council (grants EP/T00097X/1 and EP/R030081/1). This project has received funding from the European union's Horizon 2020 research and innovation programme under the Marie Skłodowska-Curie grant agreement No. 754354. H.D. acknowledges support from the European Union's Horizon 2020 research and innovation programme under the Marie Sklodowska-Curie grant agreement No. 840958.

Disclosures. D.F. and E.C. conceived the research. H.D., A.L. and J.Z. designed the experimental setup. J.Z. and A.L. performed the experiment. J.Z. and A.L. analysed the data. A.U. E.C. developed *SwissSPAD2* and H.D. developed the coincidence counting algorithm. E.C. supervised the project. All authors contributed to the manuscript.

EC: Fastree3D SA and Pi Imaging Technology SA. The remaining authors declare no conflicts of interest.

Data availability. The experimental data and codes that support the findings presented here are available from the corresponding authors upon reasonable request.

Supplemental document. See Supplement 1 for supporting content.

References

1. B. Schwarz, "Mapping the world in 3d," Nat. Photonics **4**(7), 429–430 (2010).
2. A. Velten, T. Willwacher, O. Gupta, A. Veeraraghavan, M. G. Bawendi, and R. Raskar, "Recovering three-dimensional shape around a corner using ultrafast time-of-flight imaging," Nat. Commun. **3**(1), 745 (2012).
3. G. Gariepy, F. Tonolini, R. Henderson, J. Leach, and D. Faccio, "Detection and tracking of moving objects hidden from view," Nat. Photonics **10**(1), 23–26 (2016).
4. M. O'Toole, D. B. Lindell, and G. Wetzstein, "Confocal non-line-of-sight imaging based on the light-cone transform," Nature **555**(7696), 338–341 (2018).
5. X. Liu, I. Guillén, M. La Manna, J. H. Nam, S. A. Reza, T. H. Le, A. Jarabo, D. Gutierrez, and A. Velten, "Non-line-of-sight imaging using phasor-field virtual wave optics," Nature **572**(7771), 620–623 (2019).
6. D. Faccio, A. Velten, and G. Wetzstein, "Non-line-of-sight imaging," Nat. Rev. Phys. **2**(6), 318–327 (2020).
7. A. Lyons, F. Tonolini, A. Boccolini, A. Repetti, R. Henderson, Y. Wiaux, and D. Faccio, "Computational time-of-flight diffuse optical tomography," Nat. Photonics **13**(8), 575–579 (2019).
8. C. Bruschini, H. Homulle, I. M. Antolovic, S. Burri, and E. Charbon, "Single-photon avalanche diode imagers in biophotonics: review and outlook," Light: Sci. Appl. **8**(1), 87 (2019).
9. M.-J. Sun, M. P. Edgar, G. M. Gibson, B. Sun, N. Radwell, R. Lamb, and M. J. Padgett, "Single-pixel three-dimensional imaging with time-based depth resolution," Nat. Commun. **7**(1), 12010 (2016).
10. D. Shin, F. Xu, D. Venkatraman, R. Lussana, F. Villa, F. Zappa, V. K. Goyal, F. N. Wong, and J. H. Shapiro, "Photon-efficient imaging with a single-photon camera," Nat. Commun. **7**(1), 12046 (2016).

Optics EXPRESS

11. J. Tachella, Y. Altmann, N. Mellado, A. McCarthy, R. Tobin, G. S. Buller, J.-Y. Tourneret, and S. McLaughlin, "Real-time 3d reconstruction from single-photon lidar data using plug-and-play point cloud denoisers," Nat. Commun. **10**(1), 4984 (2019).
12. C. Zhang, S. Lindner, I. M. Antolovic, J. Mata Pavia, M. Wolf, and E. Charbon, "A 30-frames/s, 252 × 144 spad flash lidar with 1728 dual-clock 48.8-ps tdcs, and pixel-wise integrated histogramming," IEEE J. Solid-State Circuits **54**(4), 1137–1151 (2019).
13. A. Ronchini Ximenes, P. Padmanabhan, M. Lee, Y. Yamashita, D. Yaung, and E. Charbon, "A modular, direct time-of-flight depth sensor in 45/65-nm 3-d-stacked cmos technology," IEEE J. Solid-State Circuits **54**(11), 3203–3214 (2019).
14. H. Seo, H. Yoon, D. Kim, J. Kim, S. J. Kim, J. H. Chun, and J. Choi, "Direct tof scanning lidar sensor with two-step multievent histogramming tdc and embedded interference filter," IEEE J. Solid-State Circuits **56**(4), 1022–1035 (2021).
15. A. C. Ulku, C. Bruschini, I. M. Antolović, Y. Kuo, R. Ankri, S. Weiss, X. Michalet, and E. Charbon, "A 512× 512 spad image sensor with integrated gating for widefield flim," IEEE J. Sel. Top. Quantum Electron. **25**(1), 1–12 (2019).
16. K. Morimoto, A. Ardelean, M.-L. Wu, A. C. Ulku, I. M. Antolovic, C. Bruschini, and E. Charbon, "Megapixel time-gated spad image sensor for 2d and 3d imaging applications," Optica **7**(4), 346–354 (2020).
17. X. Ren, P. W. Connolly, A. Halimi, Y. Altmann, S. McLaughlin, I. Gyongy, R. K. Henderson, and G. S. Buller, "High-resolution depth profiling using a range-gated cmos spad quanta image sensor," Opt. Express **26**(5), 5541–5557 (2018).
18. S. Chan, A. Halimi, F. Zhu, I. Gyongy, R. K. Henderson, R. Bowman, S. McLaughlin, G. S. Buller, and J. Leach, "Long-range depth imaging using a single-photon detector array and non-local data fusion," Sci. Rep. **9**(1), 8075 (2019).
19. C. Niclass, M. Soga, H. Matsubara, S. Kato, and M. Kagami, "A 100-m range 10-frame/s 340 ×96-pixel time-of-flight depth sensor in 0.18-μm cmos," IEEE J. Solid-State Circuits **48**(2), 559–572 (2013).
20. S. Lloyd, "Enhanced sensitivity of photodetection via quantum illumination," Science **321**(5895), 1463–1465 (2008).
21. E. Lopaeva, I. R. Berchera, I. P. Degiovanni, S. Olivares, G. Brida, and M. Genovese, "Experimental realization of quantum illumination," Phys. Rev. Lett. **110**(15), 153603 (2013).
22. Y. Zhang, D. England, A. Nomerotski, P. Svihra, S. Ferrante, P. Hockett, and B. Sussman, "Multidimensional quantum-enhanced target detection via spectrotemporal-correlation measurements," Phys. Rev. A **101**(5), 053808 (2020).
23. D. G. England, B. Balaji, and B. J. Sussman, "Quantum-enhanced standoff detection using correlated photon pairs," Phys. Rev. A **99**(2), 023828 (2019).
24. H. Defienne, M. Reichert, J. W. Fleischer, and D. Faccio, "Quantum image distillation," Sci. Adv. **5**(10), eaax0307 (2019).
25. T. Gregory, P.-A. Moreau, E. Toninelli, and M. J. Padgett, "Imaging through noise with quantum illumination," Sci. Adv. **6**(6), eaay2652 (2020).
26. P.-A. Moreau, J. Mougin-Sisini, F. Devaux, and E. Lantz, "Realization of the purely spatial einstein-podolsky-rosen paradox in full-field images of spontaneous parametric down-conversion," Phys. Rev. A **86**(1), 010101 (2012).
27. M. P. Edgar, D. S. Tasca, F. Izdebski, R. E. Warburton, J. Leach, M. Agnew, G. S. Buller, R. W. Boyd, and M. J. Padgett, "Imaging high-dimensional spatial entanglement with a camera," Nat. Commun. **3**(1), 984 (2012).
28. H. Defienne, M. Reichert, and J. W. Fleischer, "General model of photon-pair detection with an image sensor," Phys. Rev. Lett. **120**(20), 203604 (2018).
29. R. Chrapkiewicz, W. Wasilewski, and K. Banaszek, "High-fidelity spatially resolved multiphoton counting for quantum imaging applications," Opt. Lett. **39**(17), 5090–5093 (2014).
30. R. Chrapkiewicz, M. Jachura, K. Banaszek, and W. Wasilewski, "Hologram of a single photon," Nat. Photonics **10**(9), 576–579 (2016).
31. B. Eckmann, B. Bessire, M. Unternährer, L. Gasparini, M. Perenzoni, and A. Stefanov, "Characterization of space-momentum entangled photons with a time resolving cmos spad array," Opt. Express **28**(21), 31553–31571 (2020).
32. C. Ianzano, P. Svihra, M. Flament, A. Hardy, G. Cui, A. Nomerotski, and E. Figueroa, "Fast camera spatial characterization of photonic polarization entanglement," Sci. Rep. **10**(1), 6181 (2020).
33. B. Ndagano, H. Defienne, A. Lyons, I. Starshynov, F. Villa, S. Tisa, and D. Faccio, "Imaging and certifying high-dimensional entanglement with a single-photon avalanche diode camera," npj Quantum Inform. **6**(1), 94 (2020).
34. H. Defienne, J. Zhao, E. Charbon, and D. Faccio, "Full-field quantum imaging with a single-photon avalanche diode camera," Phys. Rev. A **103**(4), 042608 (2021).
35. H. Liu, D. Giovannini, H. He, D. England, B. J. Sussman, B. Balaji, and A. S. Helmy, "Enhancing lidar performance metrics using continuous-wave photon-pair sources," Optica **6**(10), 1349–1355 (2019).
36. S. Frick, A. McMillan, and J. Rarity, "Quantum rangefinding," Opt. Express **28**(25), 37118–37128 (2020).
37. X. Ren, S. Frick, A. McMillan, S. Chen, A. Halimi, P. W. R. Connolly, S. K. Joshi, S. Mclaughlin, J. G. Rarity, J. C. F. Matthews, and G. S. Buller, "Time-of-flight depth-resolved imaging with heralded photon source illumination," in *Conference on Lasers and Electro-Optics*, (Optical Society of America, 2020), p. AM3K.6.
38. L. Lydersen, C. Wiechers, C. Wittmann, D. Elser, J. Skaar, and V. Makarov, "Hacking commercial quantum cryptography systems by tailored bright illumination," Nat. Photonics **4**(10), 686–689 (2010).

Optics EXPRESS

39. K. Morimoto, M.-L. Wu, A. Ardelean, and E. Charbon, "Superluminal motion-assisted four-dimensional light-in-flight imaging," Phys. Rev. X **11**(1), 011005 (2021).
40. A. Valencia, G. Scarcelli, M. D'Angelo, and Y. Shih, "Two-photon imaging with thermal light," Phys. Rev. Lett. **94**(6), 063601 (2005).
41. L. Gasparini, M. Zarghami, H. Xu, L. Parmesan, M. M. Garcia, M. Unternährer, B. Bessire, A. Stefanov, D. Stoppa, and M. Perenzoni, "A 32×32-pixel time-resolved single-photon image sensor with 44.64μm pitch and 19.48 fill-factor with on-chip row/frame skipping features reaching 800khz observation rate for quantum physics applications," in *2018 IEEE International Solid - State Circuits Conference - (ISSCC)*, (2018), pp. 98–100.